January 2009

A biaxial stretchable interconnect with liquid-alloy-covered joints on elastomeric substrate

Kim Hyun-Joong

T. Maleki

Wei Pinghung

B. Ziaie

Hyun-Joong, Kim; Maleki, T.; Pinghung, Wei; and Ziaie, B., "A biaxial stretchable interconnect with liquid-alloy-covered joints on elastomeric substrate" (2009). *Department of Electrical and Computer Engineering Faculty Publications.* Paper 11.
http://dx.doi.org/http://dx.doi.org/10.1109/JMEMS.2008.2011118

A Biaxial Stretchable Interconnect With Liquid-Alloy-Covered Joints on Elastomeric Substrate

Hyun-Joong Kim, Teimour Maleki, Pinghung Wei, and Babak Ziaie, *Senior Member, IEEE*

***Abstract*—This paper reports a biaxial stretchable interconnect on an elastomeric substrate. To increase the stretchability of interconnects, a 2-D diamond-shaped geometry of gold on a polydimethylsiloxane substrate was adopted in which the potentially breakable points were covered with room temperature liquid alloy. Finite element model simulations were performed to identify the most vulnerable points subjected to stress concentration and optimize the design process. Simulations also indicated an optimum gold thickness and linewidth that result in a minimum stress when the substrate is stretched. Four different geometries were designed, fabricated, and characterized. These included: 1) 2-D diamond-shaped gold lines connected at circular junctions with an intersection angle of 90°; 2) 2-D diamond-shaped gold lines connected at circular junctions with intersection angles of 120° and 60°; 3) 2-D diamond-shaped gold lines separated at circular junctions with an intersection angle of 90°; and 4) 2-D diamond-shaped gold lines separated at circular junctions with intersection angles of 120° and 60°. A maximum stretchability $(\Delta L/L)$ of ∼60% was achieved for the design in which the lines and circles were separated and had intersection angles of 120° and 60°. A resistance variation of $(\Delta R/R)$ ∼30% was measured for this configuration. [2008-0248]**

***Index Terms*—Polydimethylsiloxane (PDMS), room temperature liquid alloy, smart garment, stretchable interconnect, wearable electronics.**

I. Introduction

IN THE PAST decade, flexible/conformal electronics has gained considerable attention for its applications in areas such as displays, sensitive skin, e-textile, and wearable electronics [1]–[3]. Traditional and nontraditional fabrication technologies such as screen printing, lamination, ink-jet deposition, roll-to-roll printing, solution casting, and soft lithography have been used to fabricate flexible/conformal electronics on various polymeric substrates (e.g., polyethylene terephthalate, polyethylene naphthalate, polycarbonate, and polyimide to name a few). Among the aforementioned applications, flexible displays have begun to enter the commercial market. Companies such as E.ink, LG-Phillips LCD, and Siemens have developed flexible displays currently used in various consumer and medical products. This success required a concentrated R&D effort to solve problems associated with: 1) appropriate substrate material; 2) integration of active components and interconnects; and 3) packaging [4].

A critical component of certain flexible electronic systems (e.g., wearable sensors and smart garment) which require deformation into arbitrary shapes is the multiaxial stretchable interconnect. This requires a flexible/conformal substrate that can incorporate interconnected active electronics/sensors and be able to withstand multiaxial deformation when subjected to stretching, bending, and twisting. Conductive elastomers (i.e., metal particles embedded in an elastomer) are widely used for stretchable interconnections, but the conductivity is much lower than metals and tend to change significantly with strain [5]. Several other technologies have been reported for improving the stretchability of interconnects. An example is the work by Lacour *et al.* [6] in which a thin gold film is deposited on a prestretched polydimethylsiloxane (PDMS) substrate. Upon release of the strain, a controlled sinusoidal surface pattern forms which enhances the stretchability. In another effort, Gray *et al.* [7] micromachined electroplated gold wires with a sinusoidal geometry and encapsulated them inside a thin PDMS layer capped with another PDMS. Chen *et al.* [8] designed a two-axis bendable/flexible skin using an interwoven structure on a parylene-C substrate. These methods suffer from several shortcomings such as: 1) uniaxial stretchability; 2) limited stretchability; 3) complicated fabrication process; and 4) inability to accommodate electronic components which are by nature nonstretchable.

In this paper, a simple fabrication technology is discussed in order to realize a biaxial stretchable interconnect with large strain tolerance capability using a 2-D network of diamond-shaped gold traces on an elastomeric substrate. Junctions susceptible to breakage are covered by room temperature liquid alloy, thus increasing the performance. In addition, liquid alloy reservoirs are designed to house the active surface mount component pins/legs (e.g., LED in our case), thus providing stretchability for nonstretchable components. In Sections II and III, we describe the design, simulation, and fabrication process of the 2-D diamond-shaped biaxial stretchable interconnects. In Section IV, test and characterization results are described followed by conclusions in Section V. Some of the results reported in this paper were previously presented at Transducers 2007 [9].

Manuscript received September 30, 2008. First published January 22, 2009; current version published February 4, 2009. Subject Editor C. Liu.

H.-J. Kim is with the Etch and Clean Division, Applied Materials, Sunnyvale, CA 94085 USA.

T. Maleki, P. Wei, and B. Ziaie are with Purdue University, West Lafayette, IN 47907 USA (e-mail: tmalekij@purdue.edu).

Color versions of one or more of the figures in this paper are available online at http://ieeexplore.ieee.org.

Digital Object Identifier 10.1109/JMEMS.2008.2011118

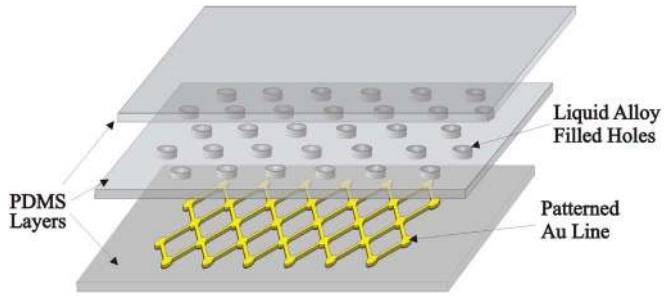

Fig. 1. Structure of the biaxial stretchable interconnect with liquid-alloy-covered joints.

II. Design and Simulation

Fig. 1 shows a schematic view of the biaxially stretchable interconnects. It consists of three PDMS layers including: 1) a base layer supporting the diamond-shaped gold traces; 2) a middle layer with liquid-alloy-filled holes; and 3) a top capping layer. Two-dimensional diamond-shaped gold traces on the PDMS layer have unique advantages including: 1) biaxial stretchablity due to their symmetrical geometry; 2) smaller stress as compare to a straight-line under the same substrate strain; and 3) lower overall electrical resistance (at the expense of a larger area). It should be mentioned that we recently presented a design with completely filled microchannels [10]. Although there are some advantages to the method described in previous approach, the current design uses less liquid alloy thus considerably reducing the cost. In addition, the theoretical analysis presented in this paper is important in designing structures with metallic thin films on elastomeric substrates and will greatly benefit the MEMS community.

It is known that free standing metallic thin films typically show a fracture strain of ~1%–2% [11]. This however can be increased to several percent if the metallic film is attached to an elastomeric substrate [12]; the reason is the ability of the elastomer to absorb part of the stress and prevent local elongation of the metallic film. As previously mentioned, the diamond shape structure allows even a greater strain through geometrical accommodation. Assuming an initial square unit cell and a strong/perfect adhesion between the metal and the elastomer, (1) can be used to represent the metallic strain

$$\varepsilon_{\text{metal}} = \frac{\sqrt{(A+\varepsilon_x A)^2 + (A-\varepsilon_y A)^2} - A\sqrt{2}}{A\sqrt{2}} \qquad (1)$$

where A is the initial length of the square, $\varepsilon_{\text{metal}}$ is the strain of the metallic diagonal line, ε_x is the substrate strain (stretch) in the x-direction, and ε_y is the substrate strain (shrinkage) in the y-direction. Assuming a Poisson's ratio of 0.5 for the elastomer, (1) can be rewritten as

$$\varepsilon_{\text{metal}} = \frac{\sqrt{(1+\varepsilon_x)^2 + (1-0.5\varepsilon_x)^2} - \sqrt{2}}{\sqrt{2}}. \qquad (2)$$

As shown, even though elastomer can be subjected to a large strain, the metallic diagonal line only experiences a fraction of that. For example, a 50% longitudinal strain in the elastomer results in only 18.6% strain in the metal.

Finite Element Analysis (COMSOL Multiphysics) simulations were performed to investigate the stress distribution in gold lines attached to the elastomeric base. Fig. 2(a) shows the finite element model (FEM) of patterned gold on PDMS substrate used in the simulations. In order to simplify the simulation, we exploited the symmetry of the structure and simulated only a quarter of the model [the white square in Fig. 2(a)]. For stretch loading simulations, force was applied in the $(x, -x)$ direction, and resulting strain in the gold lines was evaluated as a function of substrate strain. Fig. 2(b) shows the simulation results of stress distribution in the gold traces (0.7 μm thick and 30 μm wide, connecting circles have a radius of 100 μm) subjected to 20% substrate (250-μm-thick PDMS) strain. As expected, stress concentrates at the junctions between gold traces and central connecting circle (see the zoom-in view at the top of the figure). Although the value of maximum stress at the intersection regions exceeds the gold thin-film yield strength (160–220 MPa [13]), the presence of PDMS allows a larger plastic deformation than the freely suspended films. We should mention that as long as the PDMS thickness is much larger than that of the gold lines, its variation does not affect the stress distribution in the metallic conductor.

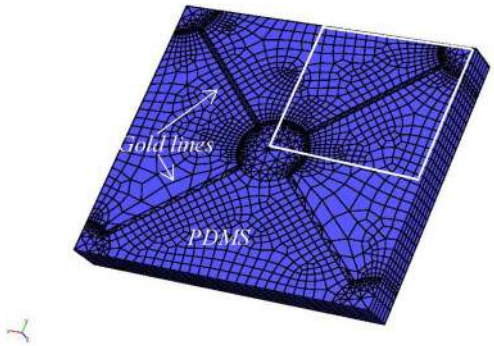

(a)

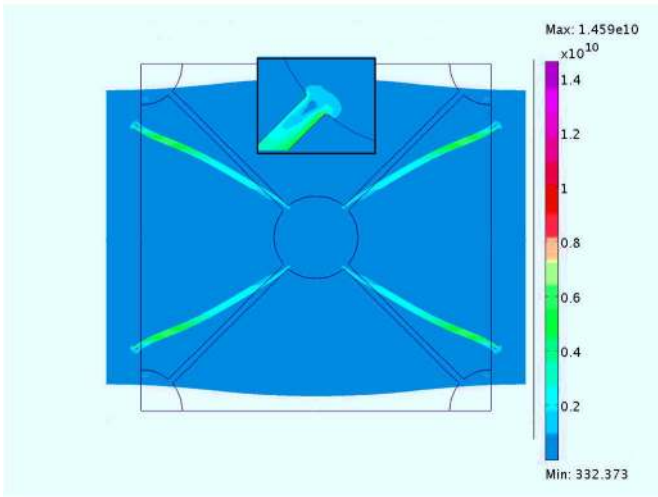

(b)

Fig. 2. (a) FEM and (b) stress distribution in gold interconnects (0.7 μm thick) on a PDMS (250 μm thick) substrate subjected to 20% strain.

In spite of the difficulty in predicting the ultimate strength of gold films bonded to an elastomeric substrate, one can gain valuable insight by simulating several different configurations/conditions. Fig. 3 shows the stress pattern for a straight line, a diagonal line connected to a circle, and a diagonal line disconnected at the maximum stress points (junction to the

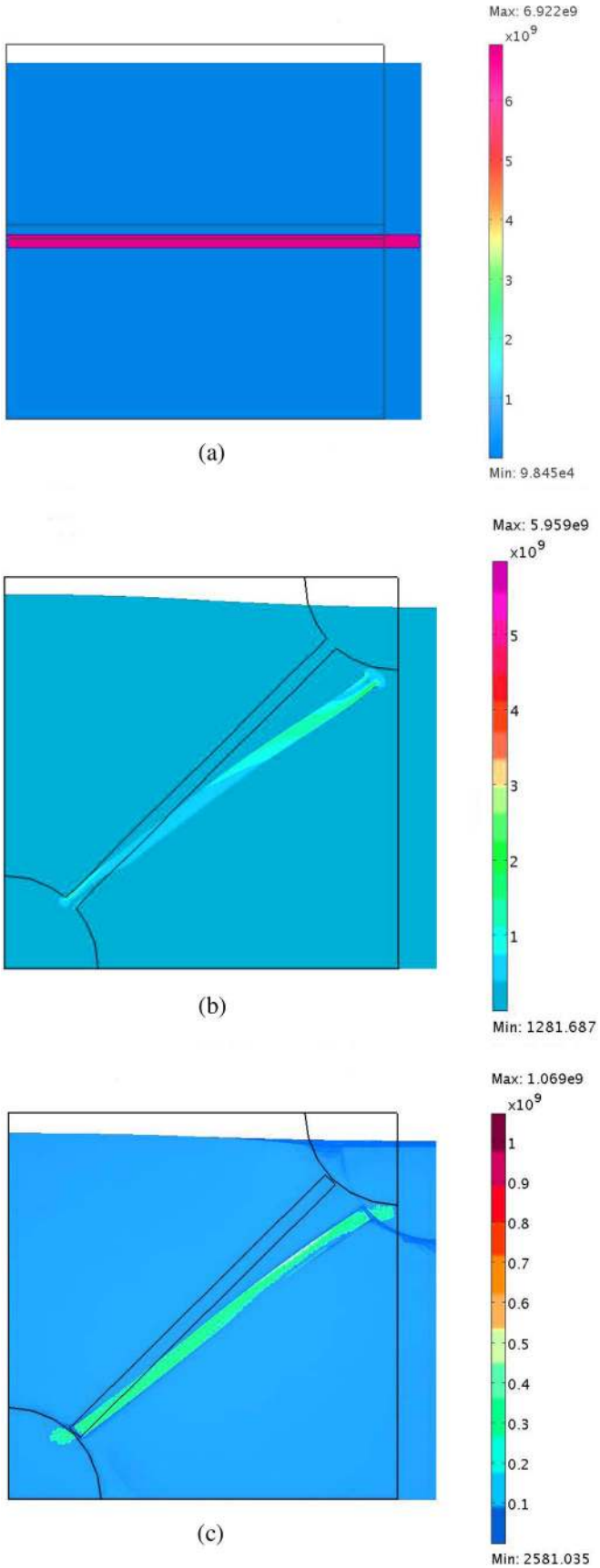

Fig. 3. Von Mises stress distribution in a 0.7-μm-thick gold thin film on a 250-μm-thick PDMS substrate for: (a) straight gold line subjected to 10% strain; (b) diagonal gold line subjected to 10% strain; and (c) broken diagonal line subjected to 10% strain.

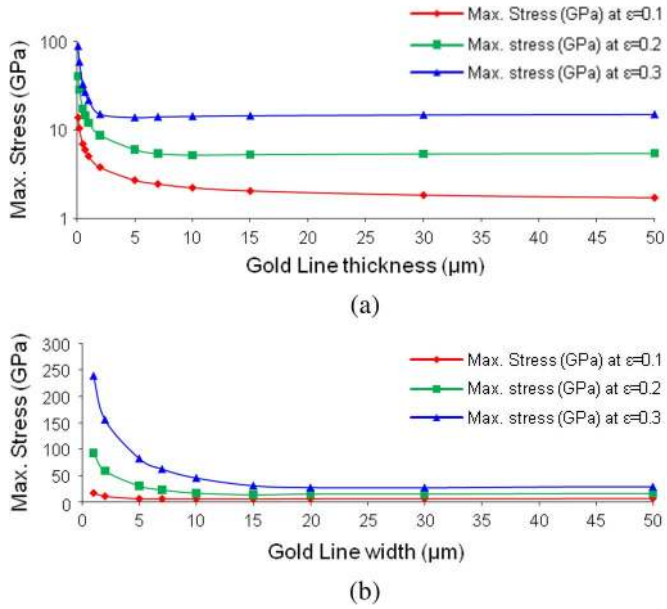

Fig. 4. (a) Maximum induced Von Mises stress in 30-μm-wide gold lines on a PDMS substrate subjected to 10%, 20%, and 30% strain versus various line thickness. (b) Maximum induced Von Mises stress in 0.7-μm-thick gold lines on a PDMS substrate subjected to 10%, 20%, and 30% strain versus various gold linewidths.

circle) all subjected to 10% strain. In all of these structures, the gold wire was assumed to be 0.7 μm thick and 30 μm wide residing on top of a 250-μm-thick PDMS substrate. As shown, in the diagonal line separated from the circle (c), the maximum stress is significantly lower than that of the straight line (7 GPa versus 1.07 GPa), whereas for the case in which the diagonal line is connected to the circle (b), stress concentration points appear at the junctions with a maximum stress of similar to the straight lines (6 GPa versus 7 GPa). This simulation clearly demonstrates the utility of using liquid metal alloy at the joints in order to maintain electrical connections after breakage of the gold lines at these junctions.

The simulation results for maximum induced stress in a diagonal line (30 μm wide) subjected to 10%, 20%, and 30% strain versus gold thickness is shown in Fig. 4(a). One can observe from the figure that maximum induced stress decreases as gold thickness increases; however, this relationship is not linear, and there is no significant decrease in the induced stress for thicknesses greater than 2.5 μm. Variation of maximum induced stress due to 10%, 20%, and 30% strain versus various linewidths for 0.7-μm-thick gold line is shown in Fig. 4(b). Again, induced stress decreases with increasing linewidths and stays constant after $\sim$15 μm. These results indicate an optimum thickness and width of 2.5 and 15 μm above which the stress will not change by increasing either the width or thickness of gold lines. It is interesting to note that the aforementioned behavior (i.e., optimum width and thickness) does not occur in straight lines (i.e., the ones that are along the strain axis). In such cases, as expected any increase or decrease in the width or thickness does not affect the stress value at a constant strain ($\sigma = E\varepsilon$, for a constant strain, stress should stay constant independent of the line cross section). The width and thickness dependence can be explained by the fact that stretched diagonal

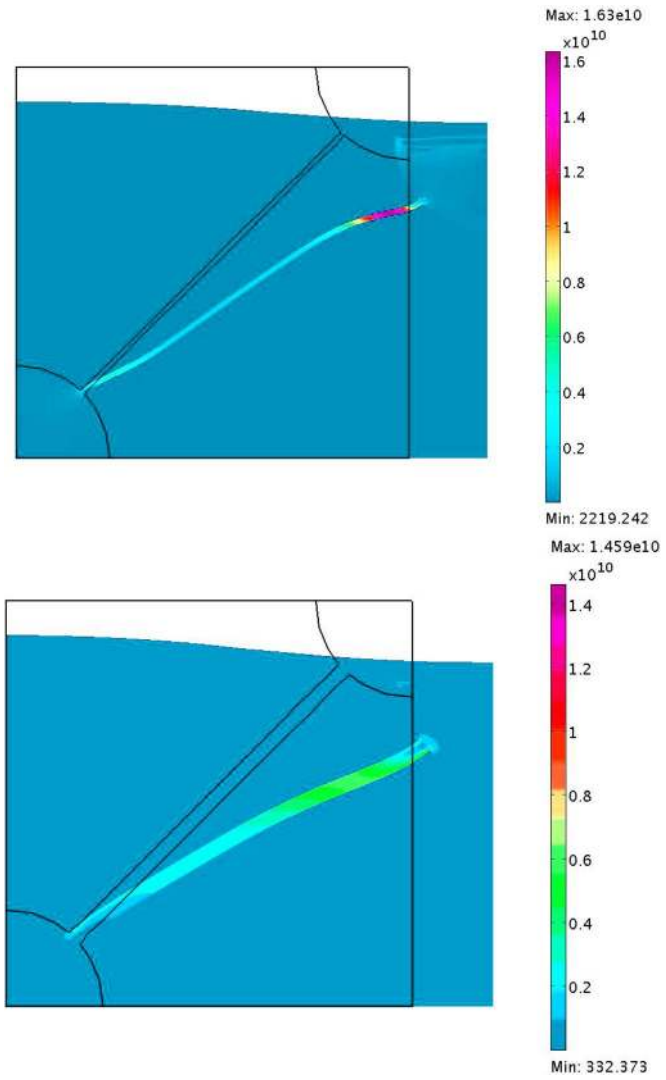

Fig. 5. Deformation of (top) 10- and (bottom) 30-μm-wide lines subjected to 20% strain.

lines deform laterally in such a way to accommodate the applied stress. Thinner and narrower lines deform more hence resulting in the aforementioned behavior. Fig. 5 shows 10- and 30-μm-wide lines subjected to 20% strain. As shown, the 10 μm line deforms to an S shape configuration with more pronounced curvatures than the 30-μm-wide line (maximum stress for the 10-μm line is $\sim$16 GPa, whereas the 30-μm line sustains a maximum stress of $\sim$5 GPa).

Finally, before discussing the fabrication process, it is instructive to calculate the total resistance of the interconnection. Fig. 6(a) shows the schematic of an interconnect segment. Resistivity of Ga/In liquid alloy (20 $\mu\Omega \cdot$ cm) is almost ten times higher than that of gold (2.2 $\mu\Omega \cdot$ cm); however, the thickness of liquid alloy circle (140 μm in our design) is 200 times larger than that of gold (0.7 μm in our design). Therefore, the calculated resistance value of the gold circle is much higher than that of liquid alloy plug ($R_1 \gg R_2$); hence, the resistance of gold circle can be ignored since it is in parallel with the liquid alloy. Gold lines and liquid alloy circles are connected in series with the resistance of the circles being much smaller than that of lines ($R \gg R_2$, alloys of 200-μm diameter

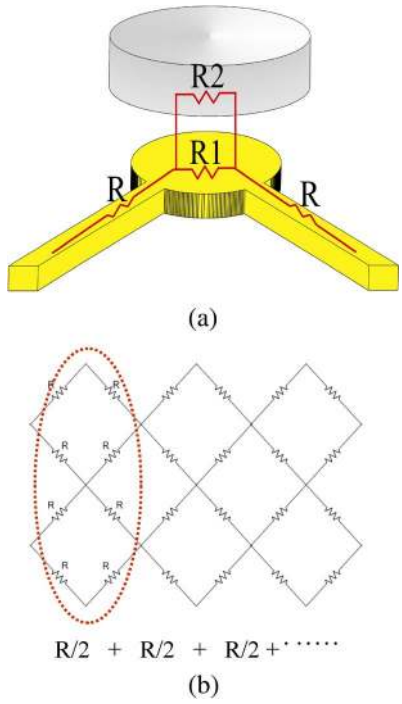

Fig. 6. Resistance network of a stretchable interconnect. (a) Resistance of each component. (b) Simplified total resistance of interconnect.

and 140-μm height as compared to 1000-μm gold straight lines having 30-μm width and 0.7-μm thickness). Fig. 6(b) shows a simplified model for the total resistance of the stretchable interconnects. As argued above, the straight gold line segments dominate the resistance with the resistance value for each segment being $R/2$. In addition, the existence of multiple paths increases the interconnects current-carrying capacity.

III. Fabrication Process

A schematic view of the fabrication process is shown in Fig. 7. A thin gold film (2000 Å) was first deposited on a silicon wafer (100 p-type). As will be seen later, this gold layer allows an easy separation of the final structure. Fresh PDMS (Sylgard 184, Dow corning, mixing ratio $= 10:1$) was prepared and spun coated on gold-deposited silicon wafer at 200 r/min for 1 min (thickness of PDMS after curing for 10 min in 90 °C oven was around 480 μm) [Fig. 7(a)]. A gold film of 0.7 μm was then directly deposited on the base PDMS layer without any adhesion layer [Fig. 7(b)]. Deposited gold film was then patterned to form 2-D diamond-shaped traces using wet etchant (TFA, Transene Company, Inc.) [Fig. 7(c)].

A second PDMS layer was separately prepared by casting onto a SU-8 (Microchem Corporation, Newton, MA) master (SU-8 2100 was spun coated onto a silicon wafer at 2000 r/min for 30 s, and patterned through standard lithography). The thickness of fabricated SU-8 master was $\sim$140 μm. Prior to PDMS casting, the SU8 surface was treated with trichlorosilane (Sigma-Aldrich Corporation) for easy release [13]. Fresh PDMS (mixing ratio $= 10:1$) was casted onto the SU-8 mold and cured at room temperature for 48 h. Lower curing temperature reduced the deformation (shrinkage) of the PDMS [14]. A transparency film was then used to form

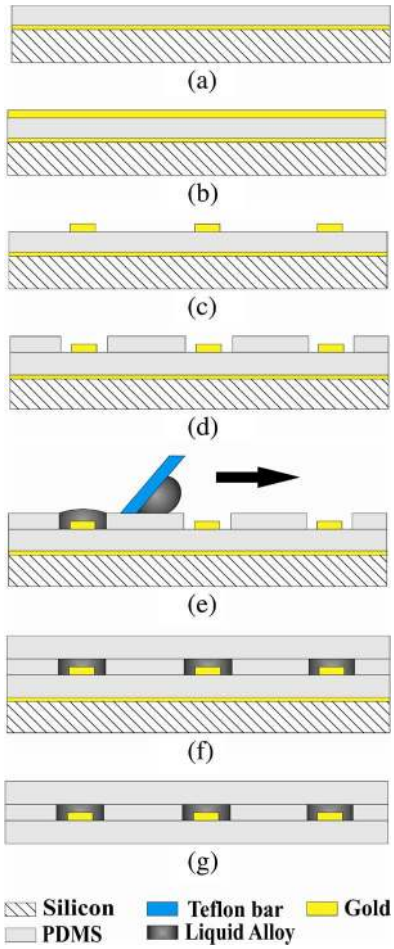

Fig. 7. Fabrication process for biaxial stretchable interconnect. (a) Gold sacrificial film and first PDMS layer deposition. (b) Gold interconnect layer deposition. (c) Gold interconnect layer patterning. (d) Bonding of the second PDMS layer with reservoir holes. (e) Screen printing of room-temperature liquid alloy onto the holes. (f) Attaching the third PDMS layer. (g) Releasing the structure from the silicon wafer.

SU-8 master/PDMS/transparency stack, which was subsequently pressurized with a heavy weight (∼2-lb steel) [15]. After curing, PDMS was detached from the SU-8 mold. A thin PDMS membrane (∼10 μm thick) still remained after peeling off even though a heavy weight was applied during the curing process. This thin PDMS membrane was removed through a wet etching (Tetrabutylammonium fluoride and N-Methylpyrrolidinone, 3:1, v/v, NMP/75% TBAF in water) step [16]. The second PDMS was bonded to the first one with the circular openings aligned to the gold line intersections on the first PDMS layer using a microscopic flip-chip aligner [Fig. 7(d)].

Each hole was then filled with room-temperature liquid alloy (Gallium/Indium $= 75.5/24.5$, Indium Corporation, liquidus temperature ≥ 15.7 °C) by screen printing technique [Fig. 7(e)]. Alternatively, one can fill the holes with an automated dispenser. The base metallic gold trace is necessary in order to fill the holes since room-temperature liquid alloy does not wet the PDMS layer. After screen printing, the surface of the second PDMS was cleaned with isopropyl alcohol to remove the liquid alloy residues. The cured third PDMS layer (1 mm thick, using a rubber spacer to control the thickness) was then attached on top of the second layer to cap the whole structure [Fig. 7(f)]. Finally, the fabricated structure was released from the silicon wafer by dripping tap water onto the Au-silicon interface [Fig. 7(g)] [17]. Fig. 8 shows an optical micrograph of the fabricated biaxial stretchable interconnect.

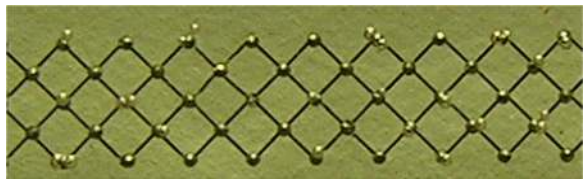

Fig. 8. Fabricated 2-D diamond-shaped stretchable interconnect.

The fabrication method outlined above was meant to demonstrate a proof of concept and can be used in small scale laboratory settings. However, one can envision an automated manufacturing process capable of roll-to-roll production of stretchable interconnects. An example would be sheets of elastomeric substrates (this does not have to be PDMS as long as it has desirable stretchability) onto which interconnect layer can be deposited through a shadow mask using a vacuum web coater. Liquid alloy holes then can be filled through an inked roller blade. Some of these methods are currently used to manufacture flexible displays and other low-cost organic electronics.

IV. Test and Characterization

A. Measurement Setup

Fabricated stretchable interconnects were bridged over two micropositioning stages (Newport 460 A, 13-mm travel range) on an optical table. Mounting blocks were placed on each end of PDMS platform and tightened with screws for stable clamping. Fixed stretchable interconnect was then stretched in one-direction by using a micromanipulator (increasing the distance between micropositioning stages). Four-point resistance measurements were performed to cancel out the resistance of external measurement wires and their contact resistance with the liquid alloy reservoirs. To measure the resistance variations, a constant current of 30 mA was applied to interconnect, and the voltage variations were recorded by a high-precision voltmeter at incremental lengths of ΔL.

B. Measured Data and Discussion

Since it is well known that Ga alloys react with many metals, before any actual stretch experiment, we measured the gold sheet resistance (ρ_s) before and after applying Ga/In liquid alloy. Four-point probe method was used for measuring sheet resistance [Fig. 9(a)]. Applied voltage was chosen to be 5 V, and the value of R_{14} was fixed at 1 kΩ. Sheet resistance can be calculated using

$$\rho_s \approx \frac{\pi}{\ln(2)} \times \frac{V_{23}}{I_{14}} = 4.523 \times \frac{V_{23}}{I_{14}} \tag{3}$$

where I_{14} is the current through R_{14}. Table I shows measured voltages, currents, and calculated sheet resistances before and

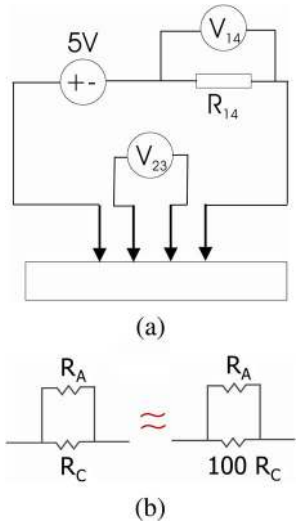

Fig. 9. (a) Four-point probe measurement setup and (b) approximate value of the interconnect resistance before and after the application of liquid alloy on the gold circle.

after applying Ga/In alloy on the gold surface. As shown, sheet resistance of gold surface after chemical reaction with Ga/In alloy increases by almost 85 times. However, the total resistance value of the interconnect is not increased since gold circles and liquid alloy circles are connected in parallel [Fig. 9(b)] ($R_{\rm C}$ is the gold circle resistance and $R_{\rm A}$ is the liquid alloy disk resistance $R_{\rm C} \gg R_{\rm A}$).

Straight gold lines were first tested to set a baseline for further measurements. Straight lines showed a maximum stretchability of less than 4%, which is typical of thin-film metallic lines on stretchable substrates. Fig. 10(a) shows fabricated interconnects without liquid alloy joints. Gold lines and circles are connected, and internal horizontal and vertical angles are 90° each. As shown, these lines are easily broken at the junctions (expected breakable points through simulation) by less than 10% strain [Fig. 10(b)]. Fig. 10(c) is an optical photograph of stretchable interconnects covering the potentially breakable points with liquid alloy showing a better strain tolerance compared to the interconnects without liquid alloy joints [Fig. 10(d)].

The lighter areas in Fig. 10(c) and (d) are unbounded regions illustrating the requirement for a complete cleaning of the surface following the screen printing process (see Fig. 8 for a defect-free bond). This can be relaxed by using a polymeric shadow mask (e.g., polyimide) with holes that can be placed on top on the PDMS prior to the screen printing and removed afterward thus minimizing the residues on the top surface. It is interesting to note that in spite of nonuniform bonding due to surface contamination, the stretchable interconnect did not fail upon repeated application of strain as shown in Fig. 10(d).

Four different types of stretchable interconnect were fabricated and characterized to compare their performance. Fig. 11 shows geometries of various interconnects. These include the following: a) lines and circles connected and having intersection angles of 90° in the x- and y-directions (**LCC 90**); b) lines and circles connected and having intersection angles of 120° and 60° in the x- and y-directions (**LCC 120**); c) lines and circles disconnected and having intersection angles of 90° in the x- and y-directions (**LCD 90**); and d) lines and circles disconnected and having intersection angles of 120° and 60° in the x- and y-directions (**LCD 120**). For the designs in which the lines are disconnected from the circular junctions, a gap of 10 μm was provided with the liquid alloy acting as the electrical connector bridging the gap. Table II shows measured initial resistance of each type of interconnects. As shown, LCD 90 shows minimum initial resistance value (3.8 Ω), because the total length of gold lines (dominant for resistance) is shorter than other structures. LCC 120 has the longest total length and shows the biggest resistance value (5.1 Ω).

Fig. 12 is the measured data for resistance variation $(\Delta R/R)$ versus strain $(\Delta L/L)$. For these experiments, three devices for each design were tested with 3–5 strain applications at each point. Fig. 12(a) shows results for LCC 90 and LCC 120 structures, as shown in Fig. 11(a) and (b). For LCC 120, a maximum strain of up to 30% can be applied with 33% resistance variations. Beyond that point, LCC 120 structures become electrically disconnected. Measured maximum stretchability of LCC 90 is ∼20% with 37% resistance variations [Fig. 12(a)]. Fig. 12(b) is the data for LCD 90 and LCD 120 structures shown in Fig. 11(c) and (d). Geometrical/structural advantage of line-circle predisconnected pattern shown in Fig. 11(c) and (d) results in a considerable improvement in stretchability. LCD 90 shows 38% resistance change for 40% strain. LCD 120 demonstrates a maximum stretchability of 60% with 35% resistance variations. Bending tests were also performed yielding a maximum resistance change of 20% for a bending angle of 90°. Further increase in bending angle resulted in permanent disconnection.

The reason for improved performance of the designs in which the line and circle junctions are separated (LCD 90 and LCD 120) can be attributed to the fact that in the connected designs (LCC 90 and LCC 120) the stress concentration points at the line-circle junctions transmit a portion of that stress to the remaining section of the line before they succumb to breakage. This is clearly visible in Fig. 10(b) (LCC 90 design) in which segments of the lines away from the junctions are also broken (notice a midline breakage on the middle left side). This stress transmission does not occur in the LCD design, hence allowing a larger strechability.

In order to evaluate the reliability of the interconnects, we subjected them to repeated strain. In particular, we were concerned about: 1) liquid alloy leakage in between the layers; 2) long term reaction of liquid alloy and gold beyond the initial application areas; and 3) overall electrical robustness. We did not notice any liquid alloy leakage after subjecting the structures to repeated strain (100 times), suggesting a strong bond between the PDMS layers (nonwettability of PDMS adds another layer of protection against leakage). We also did not measure any resistance change after several weeks of storing the interconnects at room temperature indicating no reaction between alloy and gold beyond the circular junctions onto which they were initially loaded. Finally, we strained the interconnects for 100 times and did not notice any breakage as long as the strain remained below the maximum (for example 50% of maximum strain to stay within safe limits).

TABLE I
MEASURED VOLTAGE, CURRENT, AND CALCULATED SHEET RESISTANCE

	V_{23} (mV)	I_{14} (mA)	ρ_s (Ω/□)
Au	0.5	4.9	0.46
Au &Alloy	38.9	4.57	38.49

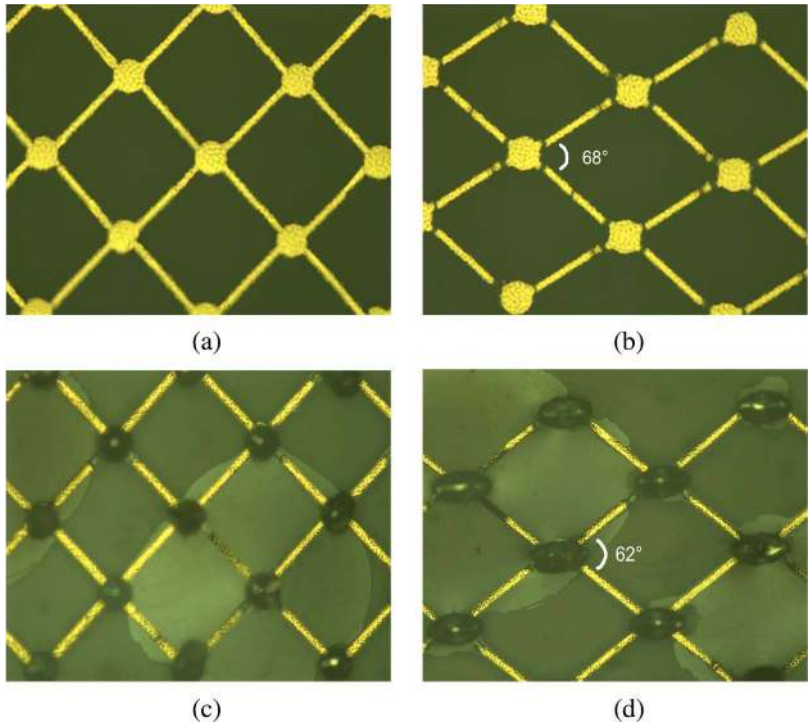

Fig. 10. Photograph of several interconnects. (a) Interconnect without liquid alloy joints (unstretched). (b) Interconnect shown in (a) broken junctions with 10% strain. (c) Interconnect with liquid alloy joints. (d) Stable connection for the interconnect shown in (c) under 20% strain.

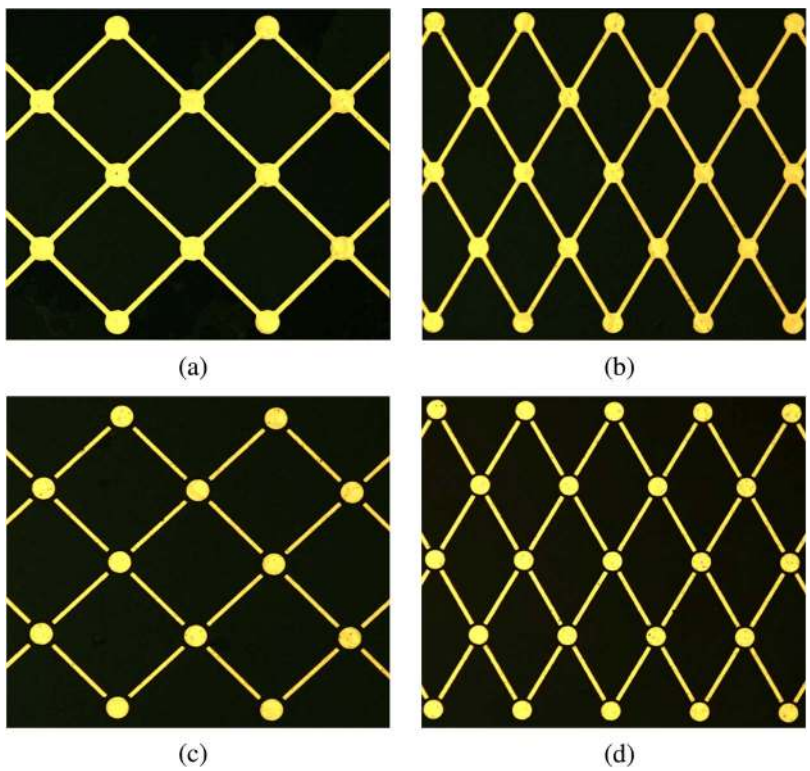

Fig. 11. Geometries of four different types of interconnects.

TABLE II
MEASURED INITIAL RESISTANCE VALUES OF EACH TYPE OF INTERCONNECT

Types	*Resistance (mean value)*
Line-circle connected, 90°-90° (x-y), 12mm length	4.6 Ω
Line-circle connected, 120°-90° (x-y), 10mm length	5.1 Ω
Line-circle disconnected, 90°-90° (x-y), 12mm length	3.8 Ω
Line-circle disconnected, 120°-90° (x-y), 10mm length	4.4 Ω

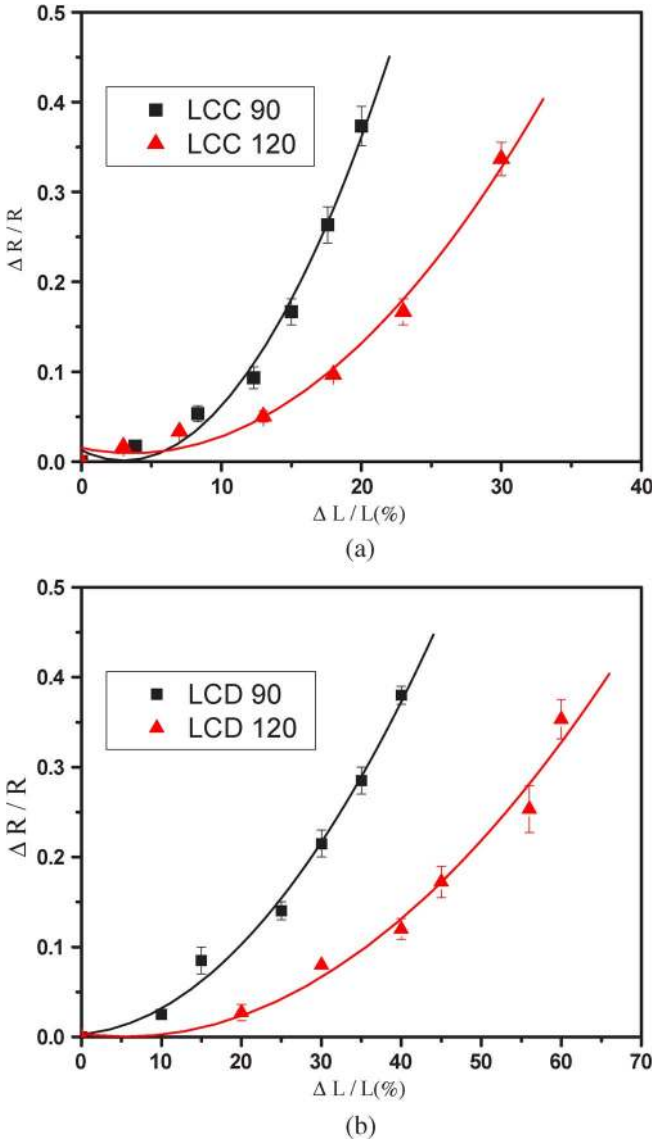

Fig. 12. Measured resistance variations versus strain. (a) LCC 90 and 120 and (b) LCD 90 and 120 (notice different x-axis scales).

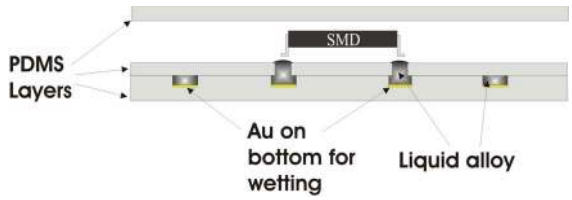

Fig. 13. Drawing of the active component integration scheme with liquid alloy reservoirs for the placement of SMD legs.

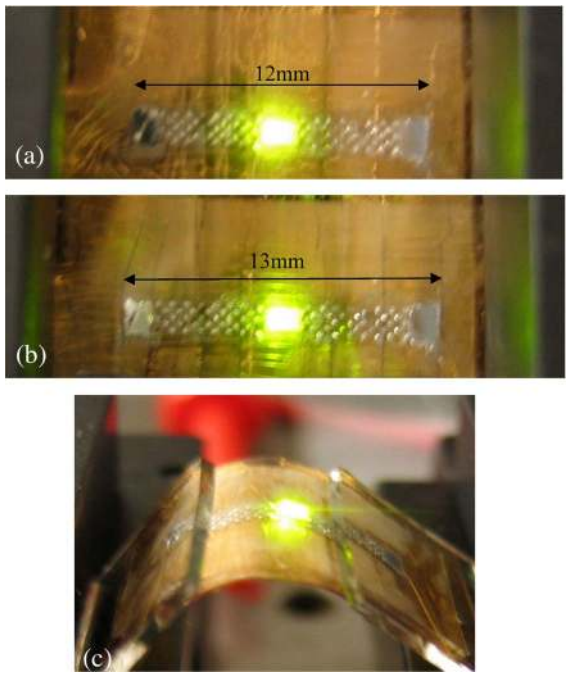

Fig. 14. LED integrated onto stretchable interconnects. (a) Before and (b) after stretching. (c) Subjected to bending.

C. Integration With Active Device

We also loaded surface mount LEDs onto the stretchable interconnect platform. Fig. 13 shows a schematic drawing of the active component integration scheme with liquid alloy reservoirs for the placement of surface mount LED pins/legs. Fabrication process is almost the same as biaxial stretchable interconnects with the surface mount LED (SML-412MW, Rohm Co., Ltd.) loaded onto the reservoirs before attaching the third PDMS capping layer. Fig. 14(a) and (b) shows LED integrated stretchable interconnect before and after the application of 8.3% strain. For PDMS substrate with active components, a lower maximum stretchability of ∼30% was observed. This is due to the constraint imposed by the limited size of the reservoirs allocated for the surface-mount LED pins/legs. If a larger stretchability for active platforms is required, a bigger reservoir can provide such a capability. Fig. 14(c) shows a bended $(\sim 60^\circ)$ stretchable interconnect with the LED (bending beyond 90° resulted in permanent disconnection). We should mention that once the surface mount component pin is dislodged from the reservoir and circuit functionality is lost, releasing the strain results in reinsertion of the pin and restoration of the functionality as long as the initial strain is not too excessive.

V. CONCLUSION

In this paper, we demonstrated a new technique to fabricate biaxially stretchable interconnects and characterized their performance. A 2-D diamond-shaped geometry of gold on a PDMS substrate was adopted in order to impart biaxial stretchability.

In addition, potentially breakable points were covered with room temperature liquid alloy to increase the functionality. Four different geometries having different intersection angles and line-circle joint structure were designed, fabricated, and characterized. A maximum stretchability of 60% with 35% resistance variations was achieved for the 2-D diamond-shaped gold lines separated at circular junctions with intersection angles of 120° and 60°. Finally, we also demonstrated the possibility of integrating active components onto the biaxial stretchable interconnect platform with stable functionality upon stretching and bending.

ACKNOWLEDGMENT

The authors would like to thank Dr. K.-S. Lim (University of Minnesota), Dr. K. Lee (Purdue University), and H. Park (Purdue University) for their valuable advice and assistance.

REFERENCES

[1] G. P. Crawford, *Flexible Flat Panel Displays*. Hoboken, NJ: Wiley, 2005.
[2] V. J. Lumelsky, M. S. Shur, and S. Wagner, "Sensitive skin," *IEEE Sensors J.*, vol. 1, no. 1, pp. 41–51, Jun. 2001.
[3] T. Martin, M. Jones, J. Edmison, and R. Shenoy, "Towards a design framework for wearable electronic textiles," in *Proc. 7th IEEE Int. Symp. Wearable Comput.*, 2003, pp. 190–199.
[4] A. Nathan and B. R. Chalamala, "Flexible electronics technology, Part II: Materials and devices," *Proc. IEEE*, vol. 93, no. 8, pp. 1391–1393, Aug. 2005.
[5] T. Tamai, "Electrical properties of conductive elastomer as electrical contact material," *IEEE Trans. Compon., Hybrids, Manuf. Technol.*, vol. CHMT-5, no. 1, pp. 56–61, Mar. 1981.
[6] S. P. Lacour, J. Jones, Z. Suo, and S. Wagner, "Design and performance of thin metal film interconnects for skin-like electronic circuits," *IEEE Electron Device Lett.*, vol. 25, no. 4, pp. 326–334, Apr. 2004.
[7] D. S. Gray, J. Tien, and C. S. Chen, "High-conductivity elastomeric electronics," *Adv. Mater.*, vol. 16, no. 5, pp. 393–397, Mar. 2004.
[8] N. Chen, J. Engel, S. Pandya, and C. Liu, "Flexible skin with two-axis bending capability made using weaving-by-lithography fabrication method," in *Proc. IEEE Int. Conf. MEMS*, Istanbul, Turkey, 2006, pp. 330–333.
[9] H.-J. Kim, M. Zhang, and B. Ziaie, "A biaxially stretchable interconnect with liquid alloy joints on flexible substrate," in *Proc. 14th Int. Conf. Solid-State Sensors Actuators*, Lyon, France, Jun. 2007, pp. 1597–1600.
[10] H. Kim, C. Son, and B. Ziaie, "A multiaxial stretchable interconnect using liquid-alloy-filled elastomeric microchannels," *Appl. Phys. Lett.*, vol. 92, no. 1, p. 011 904, Jan. 2008.
[11] H. Huang and F. Spaepen, "Tensile testing of free-standing Cu, Ag and Al thin films and Ag/Cu multilayers," *Acta Mater.*, vol. 48, no. 12, pp. 3261–3269, Jul. 2000.
[12] S. P. Lacour, J. Jones, S. Wagner, T. Li, and Z. Suo, "Stretchable interconnects for elastic electronic surfaces," *Proc. IEEE*, vol. 93, no. 8, pp. 1459–1467, Aug. 2005.
[13] K. W. Roh, K. Lim, H. Kim, and J. H. Hahn, "Poly(dimethylsiloxane) microchip for precolumn reaction and micellar electrokinetic chromatography of biogenic amines," *Electrophoresis*, vol. 23, no. 7/8, pp. 1129–1137, Apr. 2002.
[14] J.-S. Kim and D. R. Knapp, "Miniaturized multichannel electrospray ionization emitters on poly(dimethylsiloxane) microfluidic devices," *Electrophoresis*, vol. 22, no. 18, pp. 3993–3999, Oct. 2001.
[15] B. H. Jo, L. M. Van Lerberghe, K. M. Motsegood, and D. J. Beebe, "Three-dimensional micro-channel fabrication in polydimethylsiloxane (PDMS) elastomer," *J. Microelectromech. Syst.*, vol. 9, no. 1, pp. 76–81, Mar. 2000.
[16] S. Takayama, E. Ostuni, X. Qian, J. C. McDonald, X. Jiang, P. LeDuc, M. H. Wu, D. E. Ingber, and G. M. Whitesides, "Topographical micropatterning of poly(dimethylsiloxane) using laminar flows of liquids in capillaries," *Adv. Mater.*, vol. 13, no. 8, pp. 570–574, Apr. 2001.
[17] K. S. Lim, W.-J. Chang, Y.-M. Koo, and R. Bashir, "Reliable fabrication method of transferable micron scale metal pattern for poly(dimethylsiloxane) metallization," *Lab Chip*, vol. 6, no. 4, pp. 578–580, Apr. 2006.

Hyun-Joong Kim received the B.S. and M.S. degrees in electronics engineering from Inchon National University, Inchon, Korea, in 1996 and 1998, respectively, the M.S. degree in electrical and computer engineering from the University of Minnesota, Minneapolis, in 2004, and the Ph.D. degree in electrical and computer engineering from Purdue University, West Lafayette, IN, in 2008.

He is currently a Senior Process Engineer with the Etch and Clean Division, Applied Materials, Sunnyvale, CA, conducting etch process research and development in DRAM and flash memory devices. His research interests include the design and fabrication of PVDF-based ultrasound transducer arrays and fabrication technology development for stretchable interconnects for flexible electronics.

Teimour Maleki received the B.Sc. degree in biomedical engineering from Amirkabir University of Technology, Tehran, Iran, in 2000, and the M.Sc. degree in electrical engineering from the University of Tehran, Tehran, in 2003. He is currently working toward the Ph.D. degree in electrical and computer engineering at Purdue University, West Lafayette, IN.

From 2001 to 2005, he was a Research Assistant with the Thin Film Laboratory, University of Tehran, where he worked on MEMS technology (i.e., developed anisotropic etching of silicon and polymers and created membranes for sensors). Since 2006, he has been a Research Assistant with the Birck Nanotechnology Center, Purdue University. His research interests include biomedical applications of MEMS and, specifically, implantable wireless sensors.

Pinghung Wei was born in Tainan, Taiwan, in 1985. He received the B.S. degree in electrical and computer engineering from Purdue University, West Lafayette, IN, in 2006. He is currently working toward the Ph.D. degree in electrical and computer engineering at Purdue University.

His research interests include integrated flexible electrode systems and packaging techniques for neural sensing and recording.

Babak Ziaie (A'95–M'00–SM'07) received the Ph.D. degree in electrical engineering from the University of Michigan, Ann Arbor, in 1994. His dissertation was related to the design and development of an implantable single-channel microstimulator for functional neuromuscular stimulation.

From 1995 to 1999, he was a Postdoctoral Fellow and an Assistant Research Scientist with the Center for Integrated Microsystems (CIMS), University of Michigan. From 1999 to 2004, he was an Assistant Professor with the Department of Electrical and Computer Engineering, University of Minnesota, Minneapolis. Since January 2005, he has been with the School of Electrical and Computer Engineering, Purdue University, West Lafayette, IN, where he is currently an Associate Professor. His research interests include biomedical applications of MEMS and microsystems (BioMEMS), which include implantable wireless microsystems, smart polymers for physiological sensing and active flow control, micromachined interfaces with the central nervous system, biomimetic sensors and actuators, and ultrasensitive sensors for biological (molecular and cellular) applications.

Dr. Ziaie is a member of the American Association for the Advancement of Science. He was the recipient of the NSF Career Award in Biomedical Engineering (2001) and the McKnight Endowment Fund Award for Technological Innovations in Neuroscience (2002).